

2012

# Microfluidic Impedance Spectroscopy as a Tool for Quantitative Biology and Biotechnology


Ahmet C. Sabuncu  
*Old Dominion University*

Jie Zhuang

Juergen F. Kolb

Ali Beskok  
*Old Dominion University*

Follow this and additional works at: [https://digitalcommons.odu.edu/mae\\_fac\\_pubs](https://digitalcommons.odu.edu/mae_fac_pubs)

 Part of the [Biochemistry Commons](#), [Biophysics Commons](#), [Biotechnology Commons](#), [Fluid Dynamics Commons](#), [Molecular Biology Commons](#), and the [Nanotechnology Commons](#)

## Repository Citation

Sabuncu, Ahmet C.; Zhuang, Jie; Kolb, Juergen F.; and Beskok, Ali, "Microfluidic Impedance Spectroscopy as a Tool for Quantitative Biology and Biotechnology" (2012). *Mechanical & Aerospace Engineering Faculty Publications*. 59.  
[https://digitalcommons.odu.edu/mae\\_fac\\_pubs/59](https://digitalcommons.odu.edu/mae_fac_pubs/59)

## Original Publication Citation

Sabuncu, A. C., Zhuang, J., Kolb, J. F., & Beskok, A. (2012). Microfluidic impedance spectroscopy as a tool for quantitative biology and biotechnology. *Biomicrofluidics*, 6(3), 034103. doi:10.1063/1.4737121

## Microfluidic impedance spectroscopy as a tool for quantitative biology and biotechnology

Ahmet C. Sabuncu,<sup>1</sup> Jie Zhuang,<sup>2</sup> Juergen F. Kolb,<sup>2</sup> and Ali Beskok<sup>1,a)</sup>

<sup>1</sup>*Institute of Micro & Nanotechnology, Old Dominion University, Norfolk, Virginia 23529, USA*

<sup>2</sup>*Leibniz-Institute for Plasma Science and Technology (INP Greifswald), 17489 Greifswald, Germany*

(Received 14 May 2012; accepted 29 June 2012; published online 13 July 2012)

A microfluidic device that is able to perform dielectric spectroscopy is developed. The device consists of a measurement chamber that is 250  $\mu\text{m}$  thick and 750  $\mu\text{m}$  in radius. Around 1000 cells fit inside the chamber assuming average quantities for cell radius and volume fraction. This number is about 1000 folds lower than the capacity of conventional fixtures. A T-cell leukemia cell line Jurkat is tested using the microfluidic device. Measurements of deionized water and salt solutions are utilized to determine parasitic effects and geometric capacitance of the device. Physical models, including Maxwell-Wagner mixture and double shell models, are used to derive quantities for sub-cellular units. Clausius-Mossotti factor of Jurkat cells is extracted from the impedance spectrum. Effects of cellular heterogeneity are discussed and parameterized. Jurkat cells are also tested with a time domain reflectometry system for verification of the microfluidic device. Results indicate good agreement of values obtained with both techniques. The device can be used as a unique cell diagnostic tool to yield information on sub-cellular units. © 2012 American Institute of Physics. [<http://dx.doi.org/10.1063/1.4737121>]

### INTRODUCTION

Dielectric properties of cells can reveal important information. For instance, cell membrane thickness can be estimated by measuring cell suspension impedance.<sup>1</sup> Otherwise, one has to use an electron microscope, carefully fix and section cells in order to measure the cell membrane thickness. Dielectric measurements are very rapid (less than 1 s) by utilization of modern equipment that can work either in the time or frequency domains. One can also measure various quantities for cells, such as membrane capacitance and conductance by dielectric spectroscopy.<sup>2,3</sup> Consequently, instantaneous measurements of cellular compartments are possible using dielectric spectroscopy provided a physical model is available.

The dielectric properties of biological cells and tissues have been studied extensively for more than a century.<sup>4</sup> Historically, measurements of the dielectric properties of biological materials play a significant role in physiology and biophysics. Fricke conducted a theoretical and experimental analyses of the dielectric properties of red blood cell suspensions and obtained a value of 0.81 pF/cm<sup>2</sup> for the erythrocyte membrane capacitance.<sup>1</sup> He also used a value of 3 for the relative permittivity of the membrane, and derived a value for its thickness of 3.3 nm which is within a factor of two of the values currently accepted.<sup>5-7</sup> Schwan also made great contributions to the dielectric measurement and interpretation of cell suspensions and tissues.<sup>8</sup> He laid the major foundation in this field and most of his experimental designs are still used today. Many papers and text books reviewing the bulk dielectric properties of cells and tissues have been published. Schwan's 1957 review on cells and cell suspensions is one of the earliest texts

---

<sup>a)</sup>Author to whom correspondence should be addressed. Electronic mail: [abeskok@odu.edu](mailto:abeskok@odu.edu). Tel.: +1 757 683 6818. Fax: +1 757 683 3200.

on the subject.<sup>9</sup> There are other reviews by Pethig,<sup>10</sup> Stuchly,<sup>11</sup> Schwan and Foster,<sup>12</sup> Pethig and Kell,<sup>8</sup> and Foster and Schwan.<sup>13</sup> Books containing the basic knowledge and data treatment theory of this subject are written by Cole,<sup>7</sup> Grant *et al.*,<sup>14</sup> Schanne and Ceretti,<sup>5</sup> Pethig,<sup>15</sup> Grimnes and Martinsen.<sup>16</sup>

Measurement of the dielectric properties of biological materials is still an active and continuously expanding field of research. Studies in this field are increasingly leading to practical and commercial applications. For instance, the possible physiological effects caused by the absorption of non-ionizing electromagnetic radiation by tissues are becoming an area of intensive research.<sup>17</sup> The conformational changes in biological cells induced by intense pulsed electric fields were investigated before by dielectric spectroscopy.<sup>18</sup> Dielectric measurement can also be used to monitor the viability of cells.<sup>19</sup>

Microfluidics that deals with manipulation of minute amounts of fluids can provide a versatile platform for dielectric spectroscopy. Through the interplay of microfluidics and dielectric spectroscopy, cells can be individually addressed and external conditions can be fine-tuned for dielectric measurements. Recently, microfluidics has become a versatile platform that will allow multi-parameter measurement and manipulation of cells with several advantages. Gou *et al.* employed 60  $\mu\text{m}$  wide and 60  $\mu\text{m}$  deep channels with integrated coplanar gold electrodes to discriminate normal, apoptotic, and necrotic cells by measuring the resistance and capacitance at 100 kHz.<sup>20</sup> Kuettel *et al.* discriminated parasite *Babesia Bovis* infected bovine erythrocytes from uninfected and ghost erythrocytes by probing them at 8.73 MHz with coplanar electrodes.<sup>21</sup> Hua and Pennell measured the volume change of a single cell that is exposed to hypotonic environment by detecting electrical current changes, and simultaneously they recorded images of single cells by optical microscopy.<sup>22</sup> Chen *et al.* fabricated and tested a system that can simultaneously measure impedance and Young's modulus of single cells on a microfluidic platform.<sup>23</sup> Qiu *et al.* introduced a impedance based method to record the adhesion profile of cardiomyocyte in real time.<sup>24</sup>

AC electrokinetic methods stand as another way to derive cell dielectric data; however, sensitivity is limited and measurements are labor intensive.<sup>25,26</sup> Electrical impedance measurements in combination with microfluidic transport mechanisms can act to detect pathogenic bacteria.<sup>27–29</sup> Studies attempting to measure electrical impedance of single cells usually aim to discriminate certain cell types from a group of populations by probing each cell at a specific field frequency. There are also several studies attempting to detect effects of external stimuli by comparing cell suspension impedance spectra at two states rather than comparing sub-cellular properties of single cells. Therefore, most of the studies demonstrate the ability of impedance measurements in a binary fashion or can derive very limited information on cells. There is a lack of detailed data processing steps in most studies aimed to characterize cells. In this work, we provide a detailed numerical protocol to derive sub-cellular electrical properties of cells. The platform (microfluidic dielectric spectroscopy) presented here can be utilized as a tool for quantitative biology and biotechnology. In addition to the capabilities of the device and methodology that are relevant to quantitative biology, Clausius-Mossotti (CM) factor, which is a critical parameter for cell separation by dielectrophoresis (DEP), can be obtained by the device and methodology presented here. Furthermore, the effect of cellular heterogeneity on dielectric measurements is addressed for the first time in this work, where the influence of cellular heterogeneity to CM factor is presented.

In this work, a microfluidic device is developed to measure dielectric response of a small number of cells at the 1 kHz–10 MHz range, where effects due to cell membrane are prominent. The device is composed of a 750  $\mu\text{m}$  width channel and a measurement chamber that is 750  $\mu\text{m}$  in radius. Two parallel facing gold electrodes separated by 250  $\mu\text{m}$  by a polydimethylsiloxane (PDMS) chamber measure the impedance of the sample. On average, dielectric response of 5000 cells is measured in the chamber. The *main objectives* of this study are to build a microfluidic device; develop a numerical strategy using appropriate mathematical models for extraction of dielectric properties of subcellular structures; and to verify the measurements made by the microfluidic device using the time domain reflectometry (TDR) system. A numerical algorithm is developed in this study to derive quantitative information on cells. Physical models,

such as Maxwell-Wagner mixture and double shell models, are employed to derive the cell properties. Dielectric properties of standard liquids and Jurkat cell line are measured by the device. Cell membrane, cytoplasm, and nucleus properties are computed using the physical models, and the results are compared with data in the literature. Overall, the device and the methodology developed in this study is a cell diagnostic tool that is capable of characterization and sensing the effects of external stimuli.

## MATERIALS AND METHODS

### Microfabrication

The electrode geometries for the impedance device are obtained by standard photolithography techniques. Pre-cleaned microscope slides (Gold Seal micro slide, Gold Seal) are used as substrates for the device. First, glass slides are cleaned in 1 M KOH and acetone in an ultrasonic bath. The slides are then rinsed with deionized (DI) water (Simplicity, Millipore) and desiccated on a hot plate at 120 °C for 10 min. Positive photoresist (S1805, MicroChem) is spin coated on glass slides at 4000 rpm for 30 s to achieve 0.5  $\mu\text{m}$  photoresist thickness. Soft baking is applied on a hot plate at 120 °C for 1 min. The photoresist layer is exposed to 405 nm ultraviolet light (UV light source, Exoteric Instruments) for 3 s with an exposure dose of 11.74 mJ/cm<sup>2</sup>. After keeping the wafers at room temperature for 5 min, the substrates are then developed in MF24A developer for 1 min. After rinsing the slides with DI water and subsequent baking, the slides are placed in plasma cleaner for 30 s to etch excessive photoresist. 10 nm-thick Cr and 50 nm-thick Au layers are deposited on the substrate using a metal sputtering chamber (K675XD, Emitech). The electrodes of impedance chips are fabricated by applying a lift-off process in acetone. Micro-molds are manufactured by a computer numeric control machine tool. The spacers of impedance chips are obtained by casting Sylgard 184 (PDMS) silicon elastomer in machined molds. The thickness of the spacer for impedance chip is 250  $\mu\text{m}$ . The impedance chips are fabricated by aligning two electrodes on top of each other and bonding them to the PDMS spacer that is in between. In this way, a parallel plate capacitor was formed. The PDMS is functionalized by exposing it to radio frequency (RF) plasma for 1 min at 600 mTorr and 30 W. Strong binding occurred between glass and PDMS after joining them with slight pressure under a stereoscope. The fluidic inlets and outlets of microfluidic chambers were drilled by a diamond drill bit before joining the two pieces of electrodes. The schematic and picture of the impedance chip are shown in Figure 1.

### Cell lines

Dielectric spectroscopy experiments were performed on T-cell leukemia Jurkat cell lines (ATCC, Manassas, USA). Jurkat cells are grown in Roswell Park Memorial Institute Medium (RPMI; ATCC, USA). Both types of growth medium are supplemented with glutamine, penicillin, streptomycin, and 10% fetal bovine serum and cells are grown in a humidified atmosphere with 5% CO<sub>2</sub> at 37 °C. All the cells are suspended in an isotonic buffer consisting of 229 mM sucrose, 16 mM glucose, 1  $\mu\text{M}$  CaCl<sub>2</sub>, and 5 mM NaH<sub>2</sub>PO<sub>4</sub>/Na<sub>2</sub>HPO<sub>4</sub> in double distilled water (pH 7.4) for the experiments, after a washing step with isotonic buffer. The electrical conductivity of the isotonic buffers is adjusted by adding an adequate amount of phosphate buffered saline (PBS). The measurements are performed right after the suspension of cells in low conductive buffer in order to minimize the effects of the buffer. Cell size is determined by image processing the optical microscope images. Cell nucleus is marked with Hoechst fluorescent stain for sizing purposes.

### Impedance measurements

The impedance device is connected to high and low terminals to an impedance analyzer (High precision impedance analyzer, 4294 A Agilent) in a 3 terminal configuration. The microfluidic device is connected to a BNC terminal. Three aluminum plates and two wires are used as the test fixture that is between the BNC terminal and impedance analyzer. The impedance

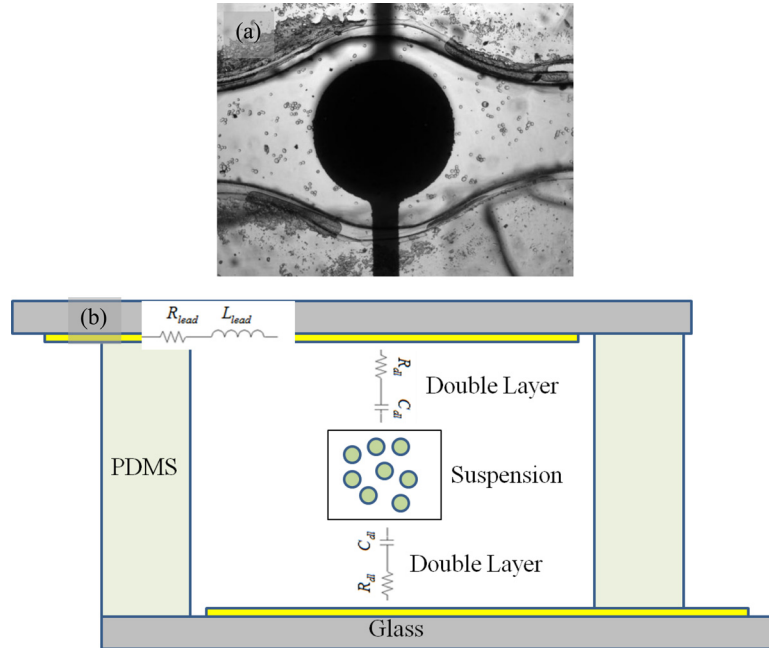


FIG. 1. Picture (a) and schematic (b) of the microfluidic device. Darker parts in the picture are electrodes. Top and bottom electrodes measure the impedance of the cell suspension in between. The schematic of the device depicts the contributions of the electrical elements.

analyzer detects impedance of the device by auto-balancing bridge method; details can be found in the impedance measurement handbook by Agilent.<sup>30</sup> Basically, while two terminals of the impedance analyzer are supplying constant voltage, the other two terminals measure current across the device. The impedance analyzer is calibrated at unknown terminals; it has a specific accuracy when the device under test (DUT) is connected to unknown terminals. However, the DUT does not always geometrically fit to the unknown terminals; several types of connectors and cables should be used between the DUT and the unknown terminals. Presence of the cables and connectors causes additional impedance sources other than DUT. They should be eliminated to yield the true impedance value for the DUT. Open, short, and load compensations were performed to obtain the true impedance spectrum of the microfluidic device. Calibration standards are used for short and open measurements. All effects caused by the presence of extra equipment in the circuit can be represented by an unknown 4-terminal circuit. Assuming that 4-terminal circuit is asymmetric, the true value of the DUT is calculated by the following formula:<sup>30</sup>

$$Z_{dut} = \frac{(Z_{sh} - Z_{xm})(Z_{sm} - Z_0)}{(Z_{xm} - Z_0)(Z_{sh} - Z_{sm})} Z_{std}, \quad (1)$$

where  $Z_{dut}$ ,  $Z_{xm}$ ,  $Z_0$ ,  $Z_{sh}$ ,  $Z_{sm}$ , and  $Z_{std}$  are corrected impedance of DUT, measured impedance of the DUT, measured impedance when the measurement terminals are open, measured impedance when the measurement terminals are short, measured impedance of the load device, and true value of the load device, respectively. Before analyzing any data obtained from the impedance analyzer, this procedure is performed to eliminate effects of the cables and the test fixture on the measured impedance. The corrected data consist of combined effects of lead resistance and inductance, stray capacitance, electrode polarization, and impedance of the suspension. The equivalent circuit that shows each element affecting the measured impedance is presented in Figure 2. Faradaic current injection is shown to be an element in the equivalent circuit for impedance measurements for DC electric fields with large electrode potentials.<sup>28</sup> Considering the frequency range and relatively low electric fields used in this study, the Faradaic effects are negligible.

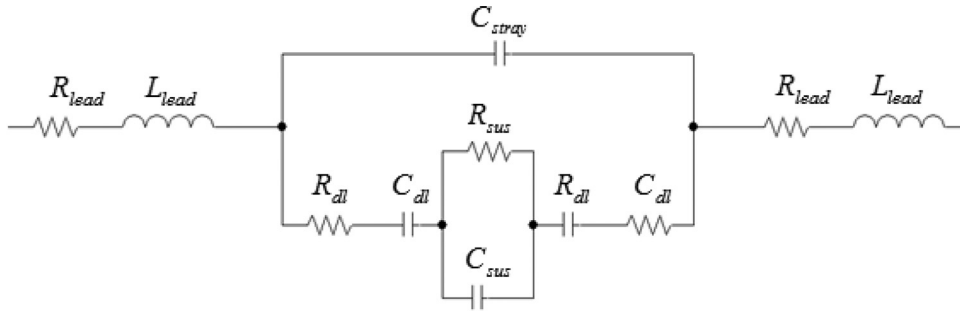


FIG. 2. Equivalent circuit of the microfluidic device. Subscripts *dl* and *sus* stand for double layer and suspension, respectively.

The first step towards fitting the data to existing models is to find the stray and unit capacitances of the device. Unit capacitance is a constant that is equal to  $kA/d$ , where  $k$  is a constant,  $A$  is the surface area of the electrodes, and  $d$  is the separation between the electrodes. Measurement of the chamber filled with DI water and an empty measurement (air) are used to determine the stray and unit capacitance values. Therefore, knowledge of exact dimensions of the device is unnecessary. Basically, the difference of reactance of DI water and air is proportional to the unit capacitance by a known constant. The values of the stray and unit capacitances are checked by measuring the impedance of salt solutions with known conductivities. The relative permittivity and conductivity values of salt solutions are checked at sufficient high frequencies in order to have no effects of electrode polarization. All complex permittivities that are determined by the fitting are derived utilizing unit capacitance. In this study, Maxwell-Wagner mixture, single, and double shell models are utilized to find cell dielectric data, as previously used by other studies.<sup>3,31</sup> The following steps are taken:

- (1) Measured impedance is fitted into a combination of constant phase element and Cole-Cole model. In this step, the effect of electrode polarization is extracted.
- (2) Cell suspension dielectric spectrum is fitted into Maxwell-Wagner mixture model. Clausius Mossotti factor is obtained.
- (3) Cell dielectric data are fitted to double shell model. Cell dielectric parameters are obtained.

Below each of these steps are described in detail. Constant phase element is used to model electrode polarization, which is given as

$$Z_{dl} = \frac{\kappa^{-1}}{(i\omega)^\alpha}, \quad (2)$$

where  $\kappa$  and  $\alpha$  are constants, and  $\omega$  is the angular frequency of the applied field. Cole-Cole model is used to model complex suspension permittivity  $\epsilon_{sus}^*$ , which is given as

$$\epsilon_{sus}^* = \epsilon_\infty + \frac{(\epsilon_s - \epsilon_\infty)}{1 + (i\omega\tau_{rel})^\beta} - i \frac{\sigma}{\omega\epsilon_0}, \quad (3)$$

where  $\epsilon_s$  and  $\epsilon_\infty$  are limiting low and high frequency values for permittivity, respectively, and  $\sigma$  is the static (DC) conductivity of the material. The inverse of the relaxation frequency is denoted by  $\tau_{rel}$ . In the above equation,  $\beta$  converges to 1 for single dispersion; whereas it converges to 0 for a dispersion occurring in infinite time. The fitting procedure varied the values of the quantities in the Cole Cole model until the difference between the model and the measurement is minimized. From the first part of the fitting, the parameters for electrode polarization ( $\kappa$  and  $\alpha$ ) and lead impedance (resistance  $R_L$  and  $L_L$ ) are determined.

The second part of the fitting uses several models to derive parameters for single cells. The electrode polarization parameters obtained from the first fitting part are used in the second part. Maxwell-Wagner mixture model is used to derive complex permittivity of a single cell from cell suspension. The model is given below

$$\varepsilon_{sus}^* = \varepsilon_m^* \frac{1 + 2pf_{cm}(\varepsilon_{cell}^*, \varepsilon_{med}^*)}{1 - pf_{cm}(\varepsilon_{cell}^*, \varepsilon_{med}^*)}, \quad (4)$$

where  $f_{cm}$  (Clausius-Mosotti factor) is,

$$f_{CM} = \frac{\varepsilon_{cell}^* - \varepsilon_{med}^*}{\varepsilon_{cell}^* + 2\varepsilon_{med}^*}. \quad (5)$$

In the above equations, *cell* and *med* indices are for cell and medium, respectively, and  $p$  is the volume fraction. In the equations, “\*” denotes complex variable.  $\varepsilon^*$  is the complex permittivity ( $\varepsilon^* = \varepsilon_r - j\sigma/\varepsilon_0\omega$ ). Maxwell Wagner model requires volume fraction of cells as an input. The volume fraction of cells is determined by a hemacytometer before the measurements.

Single and double shell models are used to fit the measured spectrum to derive parameters for subcellular compartments. The single shell model is given as

$$\varepsilon_c^* = \varepsilon_{mem}^* \frac{2(1 - \gamma_1)\varepsilon_{mem}^* + (1 + 2\gamma_1)\varepsilon_{cyt}^*}{(2 + \gamma_1)\varepsilon_{mem}^* + (1 - \gamma_1)\varepsilon_{cyt}^*}, \quad (6)$$

where subscripts *c*, *mem*, and *cyt* are for cell, membrane, and cytoplasm, respectively. The factor  $\gamma_1$  is given as,  $\gamma = (1 - t/a)^3$ , where  $t$  is the membrane thickness,  $a$  is the cell radius. Double shell model is given as

$$\varepsilon_c^* = \varepsilon_{mem}^* \frac{2(1 - \gamma_1) + (1 + 2\gamma_1)E_1}{(2 + \gamma_1) + (1 - \gamma_1)E_1}. \quad (7)$$

The parameter  $E_1$  is given as

$$E_1 = \frac{\varepsilon_{cyt}^* 2(1 - \gamma_2) + (1 + 2\gamma_2)E_2}{\varepsilon_{mem}^* (2 + \gamma_2) + (1 - \gamma_2)E_2}, \quad (8)$$

where  $\gamma_2 = (a_n/(a - t))^3$ , and  $a_n$  is the radius of the nucleus.  $E_2$  is given by

$$E_2 = \frac{\varepsilon_{ne}^* 2(1 - \gamma_3) + (1 + 2\gamma_3)E_3}{\varepsilon_{cyt}^* (2 + \gamma_3) + (1 - \gamma_3)E_3}, \quad (9)$$

where  $\gamma = (1 - t_n/a_n)^3$ ,  $E_3 = \varepsilon_{np}^*/\varepsilon_{ne}^*$ , and  $t_n$  is the nuclear envelope thickness, *np* and *ne* stands for nucleoplasm and nuclear envelope, respectively.

Cell's dielectric spectrum is obtained for frequency range 10 kHz–10 MHz. In this frequency range, dielectric spectrum is mainly affected by cell size, shape, and membrane.<sup>32</sup> Certain parameters of cells in the models, such as cytoplasm and nucleoplasm relative permittivity, are fixed in the fitting routine in order to increase the reliability of the fitting. The constants in the routine are either measurable quantities or the spectra are insensitive to their variation.<sup>31</sup> The parameters that gave minimum difference between fitted and measurement data (residual) are used to characterize cells. The fitting procedures are performed in MATLAB<sup>®</sup> (2011, Mathworks) using the nested *lsqnonlin* function that utilizes an algorithm to minimize the sum of the squares of the residuals. In order to ensure that the solution is global, 20 random starting points around the initial guess point are employed. A solution is considered correct only if multiple of starting points converge to a single solution set. This part of fitting is performed by *multistart* global optimization solver of MATLAB. The impedance data are averaged 4 times in the impedance analyzer before data acquisition. Also, all the measurements are taken at least 3 times using different suspensions.

### TDR dielectric spectroscopy

TDR is a standard method to perform dielectric spectroscopy.<sup>33,34</sup> As shown in Figure 3, an incident voltage pulse  $V_0(t)$  of known rise time and amplitude is sent into a transmission

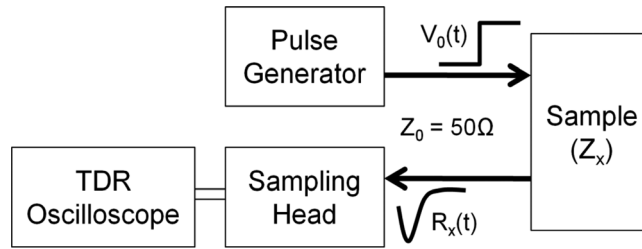


FIG. 3. Block diagram of the TDR dielectric spectroscopy system. A fast rising voltage pulse,  $V_0(t)$ , is generated by a pulse generator and applied to the sample through a coaxial cable with a characteristic impedance of  $Z_0$ . The reflected signal,  $R_x(t)$ , is digitized by a sampling head and stored in a TDR oscilloscope.

line of characteristic impedance  $Z_0$ . The transmission line is terminated with a coaxial sensor that contains the sample. Permittivity and conductivity of the sample determine its impedance,  $Z_x$ . The change in impedance at termination will result in a reflected pulse  $R_x(t)$ . The impedance of the sample,  $Z_x$ , can then be calculated by

$$Z_x = Z_0(\nu_0 + r_x) / (\nu_0 - r_x), \quad (10)$$

where  $\nu_0$  and  $r_x$  are the Fourier transforms of the time-domain incident and reflected signals,  $V_0(t)$  and  $R_x(t)$ . In practice, the reflected signal,  $R_r(t)$ , obtained for an open circuit, i.e., the empty sensor, is used instead of the incident signal  $V_0(t)$ . From the comparison of both responses (signals), the frequency dependent complex permittivity of the sample can be derived

$$\epsilon^* = \frac{1 + \rho/j\omega Z_0 C_0}{1 + \rho j\omega Z_0 C_0}, \quad (11)$$

where

$$\rho = (r_r - r_x)/(r_r + r_x), \quad (12)$$

and  $r_r$  is the Fourier transform of the empty sensor reflection.

In this study, Agilent 86100C TDR oscilloscope together with 54754A differential plug-in is used. The latter generates an incident voltage pulse with a rise time of 35 ps and amplitude of 200 mV. The same module also includes the sampling head and receives the reflected signal with an 18-GHz detection bandwidth. Samples, i.e., cell suspensions, are placed between a cut-off type termination-sensor with gold plated stainless steel electrodes. The sensor is connected to the TDR oscilloscope with a semi-rigid 3.5-mm cable of 1 m length with a characteristic impedance of 50 Ω (Agilent 8120-4948). To exclude temperature effects, the sensor is immersed in a water bath and the temperature is maintained at 25 °C with a thermostat (Julabo, San Diego, CA). The time-domain response was collected using non-uniform sampling and subsequently brought into the frequency domain by performing Laplace transform, as suggested by Hager.<sup>33</sup>

## DIELECTRIC SPECTROSCOPY RESULTS AND DISCUSSION

Impedance measurements of DI water, propylene carbonate, and empty chamber are used to determine device's geometric and stray capacitances. The geometric and stray capacitances of the microfluidic device is found as 15.91 fF and 1.45 pF, respectively. Standard salt solutions with changing conductivity are tested using the microfluidic device to evaluate device's accuracy and lead effects. Argand diagrams of fitted and measured spectra of salt solutions are given in the supporting information (Figure S1).<sup>35</sup> The computed relative permittivity and conductivity values of the salt solutions are in close proximity of nominal values. The lead resistance and inductance effects of the microfluidic device are found to be negligible.



The coefficient of variation of consecutive measurements of 217  $\mu\text{S}/\text{cm}$  salt solution permittivity and conductivity are calculated. The coefficient of variation is defined as the standard deviation over the mean of the data ( $c_v = \sigma_{std}/\mu_{mean}$ ). The coefficient of variation is a measure of the variation of impedance data between measurements. The relative change between consecutive measurements is less than 0.2% for conductivity, and less than 2% for the permittivity (Figure S2(a)).<sup>35</sup> As the variations between experiments are small, it can be deduced that the precision of the device is high.

In order to test the performance of the microfluidic device for biological cell characterization, the impedance of Jurkat cell suspension is measured. Jurkat cells, a transformed T-cell leukemia line, are non-adhesive cells of small size with relatively little cytoplasm. This implies that Jurkat cells exist in suspension naturally, which corresponds to the measurement conditions in this study. The coefficient of variation of cell impedance data over 3 successive measurements is calculated. The relative change between the measurements is less than 1% (Figure S2(b)).<sup>35</sup> This suggests high precision of the device for biological cell impedance measurements. The impedance data are fitted to physical models to derive the properties of the cell line. As described earlier, the first part of the fitting procedure includes Cole-Cole and constant phase element models to describe the cell suspensions and double layer, respectively. Limiting low and high frequency values for permittivity ( $\epsilon_s$  and  $\epsilon_\infty$ ), relaxation time ( $\tau_{rel}$ ), and DC conductivity ( $\sigma$ ) in the Cole-Cole model, (Eq. (3)) and  $\kappa$  and  $\alpha$  in the constant phase element (Eq. (2)) are set as variables while fitting the cell suspension measurement data to the models. The second part of the fitting uses  $\kappa$  and  $\alpha$  that are obtained in the first part of the fitting. Cell suspension is modeled using the Maxwell-Wagner mixture model (Eq. (4)). Two parameters governing the mixture model are cell volume fraction and CM factor. Cell volume fraction  $p$  is determined by centrifuging the cell suspension in capillary tubes, and it is set as a constant in the mixture equation.

CM factor is an important quantity for several biotechnological applications, such as DEP and electrorotation. Cells under non-uniform external electric fields exhibit positive or negative dielectrophoretic response based on their polarizability. DEP of cells is governed by CM factor. The sign of CM factor determines the direction of DEP force. Two cells of different origins are separable by DEP provided that they have different crossover frequencies.<sup>36</sup> Several types of cells having opposite dielectrophoretic responses are shown to be separable by conventional and travelling wave dielectrophoresis.<sup>37–43</sup> It was also shown previously that by recording the crossover frequencies as a function of the medium conductivity, one can obtain cell membrane capacitance and conductance.<sup>44</sup> CM factor is determined by fitting the measurement data. In Figure 4, real and imaginary parts of CM factor of Jurkat cells are plotted as a function of medium conductivity. CM factor becomes negative as medium conductivity exceeds a certain value.

Usually determination of  $p$  is prone to errors in dielectric spectroscopy, as the volume fraction is found by an indirect way, such as using hemocytometers or capillary centrifuges. Therefore, sensitivity of the CM factor to variations in volume fraction  $p$  is critical and should be computed. Using Eq. (4), the partial derivative of CM factor to  $p$  becomes

$$\frac{\partial f_{CM}}{\partial p} = \frac{-\epsilon_{sus}^{*2} - \epsilon_{sus}^* \epsilon_{med}^* + 2\epsilon_{med}^{*2}}{p^2(\epsilon_{sus}^{*2} + 4\epsilon_{sus}^* \epsilon_{med}^* + 4\epsilon_{med}^{*2})}. \quad (13)$$

Assuming experimental variation in  $p$  to be  $\delta p$ ; consequently, the variation in CM factor will be equal to,

$$\delta_{f_{CM}} = \frac{1}{p} \frac{-\epsilon_{sus}^{*2} - \epsilon_{sus}^* \epsilon_{med}^* + 2\epsilon_{med}^{*2}}{\epsilon_{sus}^{*2} + 4\epsilon_{sus}^* \epsilon_{med}^* + 4\epsilon_{med}^{*2}} \delta. \quad (14)$$

An experimentally relevant change in  $p$  will cause a variation in the CM factor equal to the value of the above expression. The above expression suggests that error in determination of

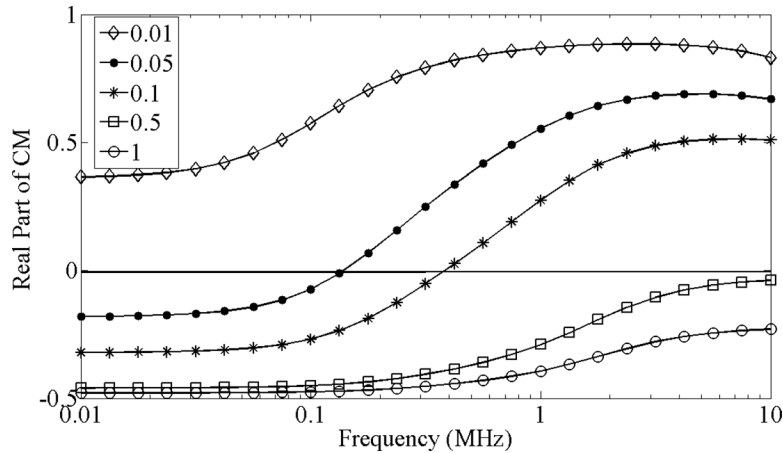


FIG. 4. Real part of CM factor for Jurkat cells as a function of frequency and at various medium conductivities. The units of the conductivity values in the inset are (S/m).

CM factor increases as volume fraction decreases. The variation in CM factor can be normalized by maximum possible value of CM factor to obtain percentile values. The above expression is plotted for  $p = 0.2$  and  $\delta = 0.1$ , and resulting real and imaginary parts of percentile variation are shown in Figure 5, which shows that the maximum error associated with the variations in volume fraction is 1%. In addition, variation in the real part is minimum around 400 kHz, whereas the variation in imaginary part is maximum around the same frequency, which is apparently around the crossover frequency for real part of CM factor at this specific external medium conductivity.

Double shell model is used to obtain  $G_{mem}$ ,  $C_{mem}$ ,  $\sigma_{cyt}$ ,  $G_{ne}$ ,  $C_{ne}$ ,  $\sigma_{np}$ ,  $\sigma_{med}$ . The following parameters are fixed to constant values before fitting the measurement data to physical models:  $a$ ,  $t$ ,  $\epsilon_{med}$ ,  $\epsilon_{cyt}$ ,  $a_n$ ,  $t_n$ ,  $\epsilon_{np}$ . Values of these constants are given in Table I. Double shell model adds two Debye-type dispersions (each for an interface) to impedance spectrum, which can be characterized by 6 parameters (two relaxation times, limiting low and high permittivity, two values of dielectric strength).<sup>3</sup> Therefore, 6 independent parameters out of 11 parameters in the double shell model are sufficient to describe the cell impedance spectrum; the rest of the parameters should be fixed in the fitting procedure. Analysis of effects of dielectric and geometrical parameters on impedance spectra revealed relatively less contribution of cytoplasm and nucleoplasm permittivity in the low frequency region in a previous study.<sup>45</sup> Considering the

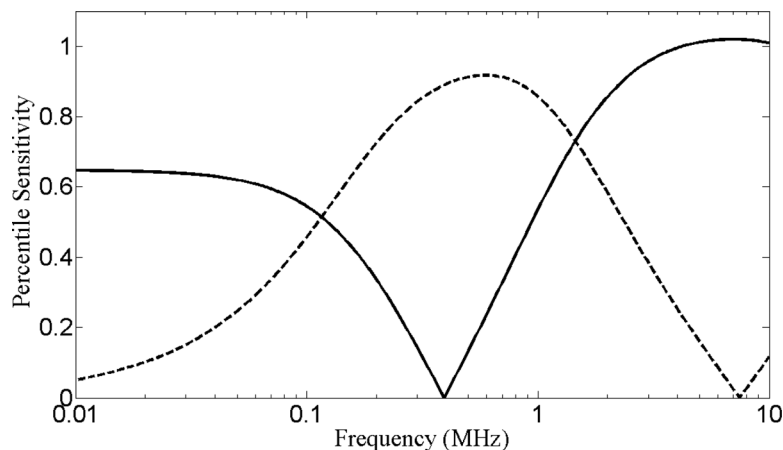


FIG. 5. Sensitivity of CM factor to 10% variation in cell volume fraction for  $p = 0.2$ . Continuous and dashed lines represent real and imaginary parts of CM factor, respectively. Cellular and medium parameters are taken from Table I.

TABLE I. Dielectric properties of Jurkat cells determined from the microfluidic and TDR system. Values in parentheses are the standard deviation.

	Microfluidic device	TDR system	Garner <i>et al.</i> <sup>47</sup>	Pethig and Talary <sup>44</sup>
$a$ ( $\mu\text{m}$ ) <sup>a</sup>	5.3	5.3	5.2	5.3
$a_n$ ( $\mu\text{m}$ ) <sup>a</sup>	4.24	4.24	3.64	...
$t$ (nm) <sup>a</sup>	7	7	7	...
$t_n$ (nm) <sup>a</sup>	40	40	14	...
$p$ (%) <sup>a</sup>	20	20	...	...
$\epsilon_{med}$ <sup>a</sup>	80	80	...	...
$\epsilon_{cyt}$ <sup>a</sup>	60	60	60	...
$\epsilon_{np}$ <sup>a</sup>	120	120	120	...
$\sigma_{med}$ (S/m)	0.099	0.147	...	...
$G_{mem}$ ( $\text{S}/\text{m}^2$ ) $\times 10^3$	5.42 (0.62)	4.48 (0.21)	0.85	...
$C_{mem}$ ( $\mu\text{F}/\text{cm}^2$ )	1.22 (0.11)	1.05 (0.025)	1.01	1.334
$\sigma_{cyt}$ (S/m)	0.32 (0.002)	0.43 (0.01)	0.25	...
$C_{ne}$ ( $\mu\text{F}/\text{cm}^2$ )	1.57 (0.01)	1.19 (0.14)	...	...
$G_{ne}$ ( $\text{S}/\text{m}^2$ ) $\times 10^3$	37.99 (8.09)	45 (5)	...	...
$\sigma_{np}$ (S/m)	0.63 (0.005)	0.82 (0.06)	0.48	...

<sup>a</sup>These values are fixed during fitting.

frequency range in this study, we fixed the cytoplasm and nucleoplasm permittivity, and geometrical parameters in the fitting procedure, and thereby only 6 parameters are left to describe Jurkat cells in the double shell model. Medium's, cell cytoplasm's, and nucleoplasm's relative permittivities ( $\epsilon_{med}$ ,  $\epsilon_{cyt}$ , and  $\epsilon_{np}$ , respectively) are set as 80, 60, and 120, respectively, in the fitting process.<sup>31</sup> The geometrical parameters are also fixed in the model. Size distribution of Jurkat cells is presented in Figure 6. The average radius ( $a$ ) of Jurkat cells is determined as  $5.3 \mu\text{m}$  from their size distribution. Diameter of the nucleus ( $a_n$ ) is set as 80% of the cell diameter, as determined by image processing of Hoechst dye stained cell. Cell membrane ( $t$ ) and nuclear membrane ( $t_n$ ) thicknesses are taken as 7 and 40 nm, respectively. Cell membrane and nuclear envelope permittivity and conductivity ( $\epsilon_{mem}$ ,  $\sigma_{mem}$ ,  $\epsilon_{ne}$ ,  $\sigma_{ne}$ ), cytoplasm and nucleoplasm conductivity ( $\sigma_{cyt}$ ,  $\sigma_{np}$ ) are set to change in the routine. The cell parameters obtained from the fitting procedure are given in Table I. Standard deviation is calculated from the data obtained at consecutive measurements, and its value for each fitting variable in the double shell model is

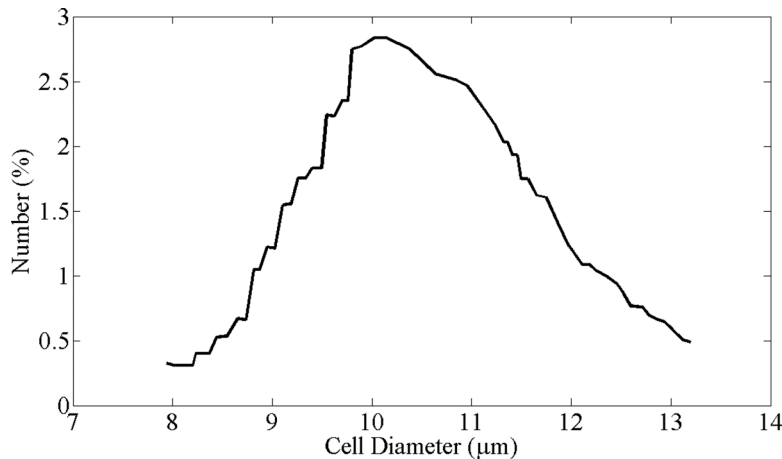


FIG. 6. Size distribution of Jurkat cells determined using Coulter counter.

given in Table I. Membrane capacitance and conductance in Table I are calculated by  $C_{mem} = \epsilon_{mem}\epsilon_0/t$  and  $G_{mem} = \sigma_{mem}/t$ , respectively.

The permittivity and conductivity spectra built using the values obtained from the fitting procedure and measurement data of the Jurkat cell suspension are plotted in Figures 7(a) and 7(b), respectively. The figure also shows the suspension permittivity and conductivity after extracting the effects of electrode polarization. The effect of electrode polarization is clearly seen at low frequencies (below 200 kHz), which dominates the cell suspension data in this range. Therefore, double layer ( $\alpha$ ) polarization of cells is not observable from the measurements. The interfacial ( $\beta$ ) dispersion, which is due to the polarization at cell boundaries, is visible after 200 kHz. The relative permittivity drops with the onset of  $\beta$  dispersion, and it continues to drop up to 10 MHz. The percentile errors of the relative permittivity are higher than those of conductivity. In the low frequency region (below 200 kHz), the percentile error is around 5% while the percentile error in conductivity in this region is around 0.1%. After 200 kHz, the percentile errors alternate between  $\pm 2\%$  and  $\pm 0.5\%$  for relative permittivity and conductivity, respectively. The errors are mainly due to models inability to describe experimental data's dispersion characteristics. Both of the percentile errors are higher around the onset and end of the  $\beta$  dispersion range (at around 200 kHz and 2 MHz, respectively). The details of the percentile errors of modeled permittivity and conductivity spectra relative to the measurement data are given in the supporting information Figure S3.<sup>35</sup> In addition, single shell model is used to obtain parameters for cell membrane in order to compare the effectiveness of the double and single shell models. In the fitting with single shell model, cell cytoplasm conductivity and relative permittivity are set to 0.5 S/m and 60, respectively. Cell suspension's relative permittivity and conductivity spectra

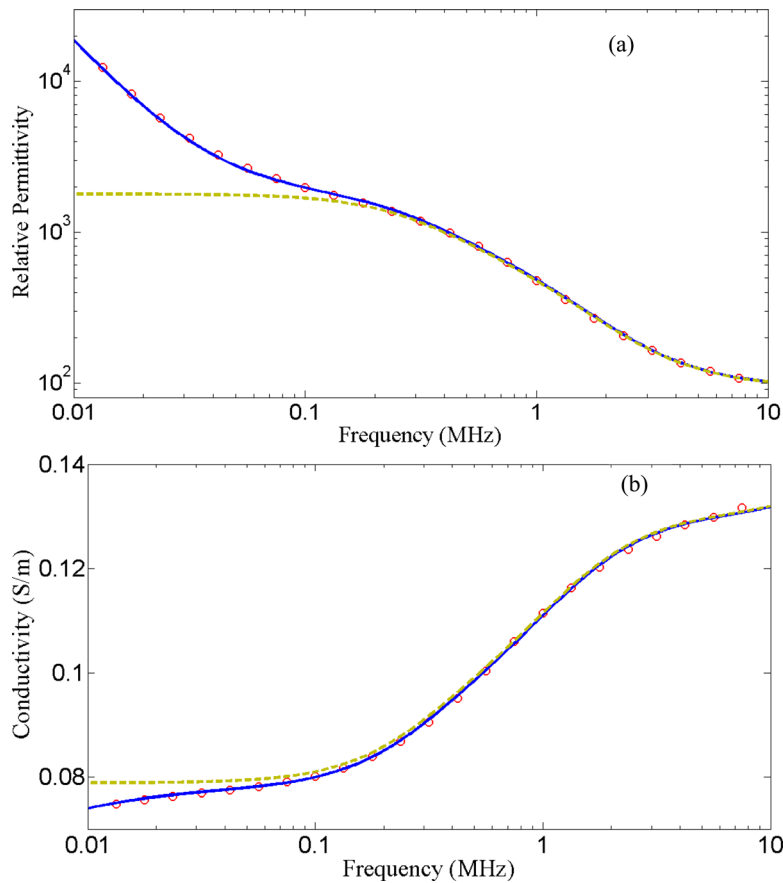


FIG. 7. The measured (circular markers) and modeled (continuous line) permittivities (a) and conductivity (b) data for Jurkat cell suspension. Dashed line represents the impedance spectrum of suspension after electrode polarization effects are removed.

built using single shell model are shown in Figure S4.<sup>35</sup> Cell parameters obtained from the single shell fitting is listed in Table S1.<sup>35</sup> The single shell model does not describe the dispersion as accurately as the double shell model. Consequently, the percentile errors are larger in single shell model, which are shown in Figure S5.<sup>35</sup>

The fitting algorithm used in this study to extract dielectric properties finds the local minima of the fitting function. This potentially allows several sets of variables to satisfy the convergence criteria. A global optimization routine is employed to ensure convergence to a single global solution. The simulation is started at 100 random points around the initial guess point of each variable. The local solver is run for all starting points. All of the local runs converged to a single solution point, namely to the global solution. The single global solution is the same as the local solution presented previously. The contour map of the square root of sum of the residuals (L2 norm) is plotted as a function of the membrane conductivity and relative permittivity in Figure S6.<sup>35</sup> The starting points and the global solution at membrane relative permittivity and conductivity plane are shown in Figure S6 (Ref. 35) by dots and a star, respectively. In this figure, all other fitting parameters are fixed to their values that are obtained by global optimization. Convergence of the algorithm to a global solution ensures its uniqueness. 95% confidence limits of each fitting parameter in the double shell model are given in Table II to demonstrate the reliability of the fit. According to Table II, upper and lower limits of 95% confidence levels of membrane capacitance and the conductance deviates about 2% and 1% from the nominal values, respectively.

In order to verify the results obtained by the microfluidic device, Jurkat cell parameters are measured with TDR system. The cell parameters obtained by TDR are shown in Table I. Cell membrane permittivity and conductivity values obtained by TDR are  $1.05 \mu\text{F}/\text{cm}^2$ ,  $4.48 \times 10^3 \text{ S}/\text{m}^2$ , respectively. According to Table I, there is about 14% variation in membrane permittivity and about 17% variation in membrane conductivity between the quantities obtained from the TDR system and microfluidic device. Standard deviations fall into 9% and 11% of the mean membrane capacitance and conductance values obtained by microfluidic spectroscopy, respectively. These variations may be due to poor sampling of cell count or variances between the cell phenotypes. In TDR measurements, the actual sample in the system could not be counted due to geometric and material restrictions; instead aliquots from the cell suspension are counted using a hemacytometer. This condition brings further errors to the TDR measurement. In addition, even though two aliquots from the same cell suspension are thought to be structurally and functionally identical, there might be differences pertaining to cellular heterogeneity. These facts could have contributed to the differences in cell membrane capacitance and conductance. Cells exhibit a dynamic behavior once they are suspended in low conductive buffers that are used for electrical manipulations and measurements. We observed significant temporal changes in extracellular conductivity in impedance measurements. The same trend was also observed by Gascoyne *et al.*, and the change in extracellular medium was attributed to leakage of K cations from the cytoplasm.<sup>46</sup> These effects should have contributed to the difference in the cytoplasm conductivities obtained by both techniques. Apart from these facts, precise determination of stray capacitance is not possible for both techniques, since each sample will cause different stray effects, precise determination of stray capacitance is impossible. Also, the equivalent circuit proposed in this study is only an approximation, ensuring good fit to the measurement data. However, several other unknown effects could play a role in the establishment of the equivalent circuit. Furthermore, Jurkat cell dielectric data are compared to those obtained in

TABLE II. 95% confidence intervals for fitting parameters.

	$C_{\text{mem}} (\mu\text{F}/\text{cm}^2)$	$G_{\text{mem}} (\text{S}/\text{m}^2) \times 10^{-3}$	$\sigma_{\text{cyl}} (\text{S}/\text{m})$	$C_{\text{nc}} (\mu\text{F}/\text{cm}^2)$	$G_{\text{nc}} (\text{S}/\text{m}^2) \times 10^{-3}$	$\sigma_{\text{np}} (\text{S}/\text{m})$
Mean value	1.15	4.97	0.321	1.59	43.72	0.635
Upper value	1.13	4.94	0.324	1.56	44.93	0.642
Lower value	1.16	5.01	0.319	1.61	42.51	0.628

other studies. Jurkat cell data from the studies of Pethig and Talary and Garner *et al.* are shown in Table I.<sup>44,47</sup> All studies report similar cell membrane capacitance; however, membrane conductance from the study of Garner *et al.* is several orders lower than our data and the data from other reported normal and malignant T-cell dielectric data.<sup>3,31</sup> Pethig and Talary's study does not report any membrane conductance data. Their measurement technique includes determination of dielectrophoretic crossover frequency measurement and agreement of the data with this study shows applicability of impedance measurements in dielectrophoresis.

Morphological heterogeneity of Jurkat cells might play a role on dielectric spectra. One aspect of this heterogeneity is clearly visible in Figure 6, where size distribution of Jurkat cells is plotted. More generally, the heterogeneity of Jurkat cells might result in distribution of relaxation times. Size variation is the most significant observable cellular heterogeneity parameter. Moreover, Cole-Cole model used in the first part of the fitting procedure assumes symmetrical distribution of relaxation times around a mean; however, there is no such assumption in the double shell model. In order to account for the heterogeneity of Jurkat cells and distribution of relaxation times, a distribution of CM factor is assumed for the fitting. Therefore, Eq. (4) becomes

$$\epsilon_{sus}^* = \epsilon_m^* \sum_{i=1}^k \frac{1 + 2p r_i f_{cm,i}}{1 - p r_i f_{cm,i}}, \quad (15)$$

where  $r_i$  is the relative contribution of sub-population  $i$  to the overall volume fraction  $p$ . The characteristic relaxation time,  $\tau_\beta = (\epsilon_{cell} + 2\epsilon_{med}) / (\sigma_{cell} + 2\sigma_{med})$ , is set to have a normal distribution. The relative contribution  $r_i$  is also set to have normal distribution. The mean of the characteristic frequency is constructed from the original double shell solution. Only standard deviation ( $\sigma$ ) is set to vary in the fitting. The standard deviation is varied until the corresponding normalized error of the fitting is the same as the normalized error of the original double shell model. The details are given in Figure S7.<sup>35</sup> The heterogeneity in the cell line can be estimated as 0.37%, which is found by dividing the standard deviation by the mean value of characteristic frequency. The fitted impedance spectra and the percentile errors assuming this distribution are given in Figures S8 and S9, respectively.<sup>35</sup> The quality of the fit and errors are the same as those corresponding to double shell model with no distribution of relaxation times. The CM factors at  $\pm 3\sigma$  and mean of characteristic frequency are plotted in Figure 8. According to the figure, crossover of a single cell can vary between 1.09 and 1.2 MHz at 0.35 S/m medium conductivity. In order to define two cell lines as separable by DEP, this range should not overlap for those of the two cell lines.

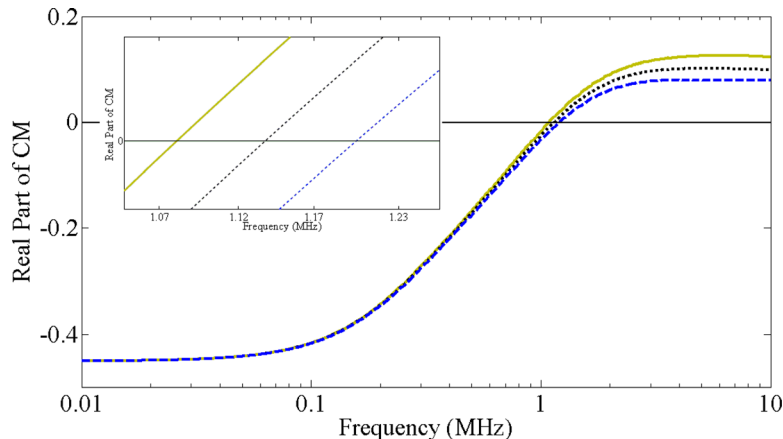


FIG. 8. Effect of cell heterogeneity on CM factor at 0.35 S/m medium conductivity. Continuous, dashed, and dotted lines present maximum, minimum, and average CM factors, respectively.

## CONCLUSIONS

In this paper, a microfluidic device that is capable of performing dielectric spectroscopy and can function as a cell diagnosis tool is presented. The device is fabricated using standard photolithography and soft-lithography tools. A cell suspension is fed into the device from the fluidic inlet. An equivalent circuit is given to describe the contributions of various elements that affect the cell suspension data. Measurements of standard liquids with known permittivity and conductivity and empty device are utilized to determine the magnitude of parasitic effects and geometric capacitance. Jurkat cells, a T-cell leukemia line, are tested to evaluate the capability of the device for cell characterization. Maxwell-Wagner mixture and double shell models are utilized to model cell suspension and a single cell, respectively. Electrode polarization effects are described by constant phase element model. A fitting algorithm is used to determine model parameters that ensure a good fit to measurement data. The fitting algorithm also ensured the presence of one global solution by employing multiple starting points for fitting. The data are further verified with the results from a TDR system. The microfluidic device and numerical methodology presented here are able to derive sub-cellular properties of cells with high reliability.

A unique advantage of microfluidic devices is the reduction of number of cells that are entrained in the measurement chamber. Conventional fixtures for dielectric spectroscopy hold around thousand folds greater number of cells. This in turn yields the microfluidic chambers to operate at lower costs at the same precision and accuracy. Microfluidic impedance measurement chambers can yield quantitative information on biological effects of various stimuli, and thus it serves as an important tool for quantitative biology, where dielectric properties of cells provide quantitative information on cell's biological state. Such measurements can make a critical impact on fundamental biology once combined with other microfluidic elements that can sustain controlled chemical and electromagnetic environments in the device. The devices can be connected to an upstream component that performs a different task, for example, introduction of a chemical or electromagnetic stimulus. Stimuli can also be introduced at the measurement chamber, thus, making recording of instantaneous response of cells possible. This manuscript introduces a simple microfluidic test fixture for dielectric spectroscopy and relevant data processing methodology to obtain quantitative information on biological cells. The electrodes can be arranged in different formations using the same fabrication techniques, yielding optical observation and broader functionality. Long term cell culture experiments in the chamber can also be possible by utilization of a suitable pH buffering system. In addition, the measurement methodology and the device presented in this study can serve as a precursor for DEP studies of cells, since it can determine the CM factor of cells, which is critical for dielectrophoresis applications. For instance, several previous studies attempted to utilize DEP for cancer research including separation and isolation of circulating tumor cells (CTCs);<sup>48–50</sup> in this regard, CM measurements of CTCs by dielectric spectroscopy can help researchers to design effective and rapid DEP sorters.

<sup>1</sup>H. Fricke, *J. Gen. Physiol.* **9**, 137–152 (1925).

<sup>2</sup>Y. Feldman, I. Ermolina, and Y. Hayashi, *IEEE Trans. Dielectr. Electr. Insul.* **10**, 728–753 (2003).

<sup>3</sup>I. Ermolina, Y. Polevaya, Y. Feldman, B. Ginzburg, and M. Schlesinger, *IEEE Trans. Dielectr. Electr. Insul.* **8**, 253–261 (2001).

<sup>4</sup>G. Markx and C. Davey, *Enzyme Microb. Technol.* **25**, 161–171 (1999).

<sup>5</sup>O. Schanne and E. Ceretti, *Impedance Measurements in Biological Cells* (John Wiley & Sons, 1978).

<sup>6</sup>D. Kell and C. Harris, *Electromagn. Biol. Med.* **4**, 317–348 (1985).

<sup>7</sup>K. Cole, *Membranes, Ions, and Impulses* (University of California Press, Berkeley, 1972).

<sup>8</sup>R. Pethig and D. Kell, *Phys. Med. Biol.* **32**, 933–970 (1987).

<sup>9</sup>H. Schwan, *Adv. Biol. Med. Phys.* **5**, 147 (1957).

<sup>10</sup>R. Pethig, *IEEE Trans. Electr. Insul.* **EI-19**(5), 453–474 (1984).

<sup>11</sup>M. Stuchly, *J. Microwave Power* **15**, 19–26 (1980).

<sup>12</sup>H. Schwan and K. Foster, *Proc. IEEE* **68**, 104–113 (1980).

<sup>13</sup>K. Foster and H. Schwan, *CRC Crit. Rev. Biomed. Eng.* **17**, 25–104 (1989).

<sup>14</sup>E. Grant, R. Sheppard, and G. South, *Dielectric Behaviour of Biological Molecules in Solution* (Clarendon, Oxford, 1978).

<sup>15</sup>R. Pethig, *Dielectric and Electronic Properties of Biological Materials* (Wiley, New York, 1979).

<sup>16</sup>S. Grimnes and O. Martinsen, *Bioimpedance and Bioelectricity Basics* (Academic, 2008).

<sup>17</sup>A. Christ, A. Klingenbock, T. Samaras, C. Goiceanu, and N. Kuster, *IEEE Trans. Microwave Theory Tech.* **54**, 2188–2195 (2006).

- <sup>18</sup>J. Zhuang, W. Ren, Y. Jing, and J. F. Kolb, *IEEE Trans. Dielectr. Electr. Insul.* **19**, 609–622 (2012).
- <sup>19</sup>P. Patel and G. Markx, *Enzyme Microb. Technol.* **43**, 463–470 (2008).
- <sup>20</sup>H.-L. Gou, X.-B. Zhang, N. Bao, J.-J. Xu, X.-H. Xia, and H.-Y. Chen, *J. Chromatogr. A* **1218**, 5725–5729 (2011).
- <sup>21</sup>C. Küttel, E. Nascimento, N. Demierre, T. Silva, T. Braschler, P. Renaud, and A. G. Oliva, *Acta Trop.* **102**, 63–68 (2007).
- <sup>22</sup>S. Z. Hua and T. Pennell, *Lab Chip* **9**, 251–256 (2009).
- <sup>23</sup>J. Chen, *Biomicrofluidics* **5**, 014113 (2011).
- <sup>24</sup>Y. Qiu, R. Liao, and X. Zhang, *Anal. Chem.* **80**, 990–996 (2008).
- <sup>25</sup>M. Nikolic-Jaric, S. F. Romanuik, G. A. Ferrier, T. Cabel, E. Salimi, D. B. Levin, G. E. Bridges, and D. J. Thomson, *Biomicrofluidics* **6**, 024117 (2012).
- <sup>26</sup>U. Lei, P.-H. Sun, and R. Pethig, *Biomicrofluidics* **5**, 044109 (2011).
- <sup>27</sup>J. Wu, Y. Ben, D. Battigelli, and H.-C. Chang, *Ind. Eng. Chem. Res.* **44**, 2815–2822 (2005).
- <sup>28</sup>J. Wu, Y. Ben, and H. C. Chang, *Microfluid. Nanofluid.* **1**, 161–167 (2005).
- <sup>29</sup>S. Sengupta, D. A. Battigelli, and H.-C. Chang, *Lab Chip* **6**, 682–692 (2006).
- <sup>30</sup>M. Honda, *A Guide to Measurement Technology and Technique* (Agilent Technologies, USA, 2009).
- <sup>31</sup>Y. Polevaya, I. Ermolina, M. Schlesinger, B.-Z. Ginzburg, and Y. Feldman, *Biochim. Biophys. Acta-Biomembr.* **1419**, 257–271 (1999).
- <sup>32</sup>K. Asami, *J. Non-Cryst. Solids* **305**, 268–277 (2002).
- <sup>33</sup>N. Hager III, *Rev. Sci. Instrum.* **65**, 887 (1994).
- <sup>34</sup>N. Hager III and R. Domszy, *J. Appl. Phys.* **96**, 5117 (2004).
- <sup>35</sup>See supplementary material at <http://dx.doi.org/10.1063/1.4737121> for additional information.
- <sup>36</sup>R. Pethig, *Biomicrofluidics* **4**, 022811–022835 (2010).
- <sup>37</sup>P. R. C. Gascoyne, X.-B. Wang, Y. Huang, and F. F. Becker, *IEEE Trans. Ind. Appl.* **33**, 670–678 (1997).
- <sup>38</sup>Y. Kang, B. Cetin, Z. Wu, and D. Li, *Electrochim. Acta* **54**, 1715–1720 (2009).
- <sup>39</sup>A. C. Sabuncu, J. A. Liu, S. J. Beebe, and A. Beskok, *Biomicrofluidics* **4**, 021101–021107 (2010).
- <sup>40</sup>S. Park, Y. Zhang, T.-H. Wang, and S. Yang, *Lab Chip* **11**, 2893–2900 (2011).
- <sup>41</sup>S. Park, M. Koklu, and A. Beskok, *Anal. Chem.* **81**, 2303–2310 (2009).
- <sup>42</sup>I. F. Cheng, V. E. Froude, Y. Zhu, H.-C. Chang, and H.-C. Chang, *Lab Chip* **9**, 3193–3201 (2009).
- <sup>43</sup>Z. Gagnon, J. Mazur, and H. C. Chang, *Lab Chip* **10**, 718–726 (2010).
- <sup>44</sup>R. Pethig and M. S. Talary, *IET Nanobiotechnol.* **1**, 2–9 (2007).
- <sup>45</sup>I. Ermolina, Y. Polevaya, and Y. Feldman, *Eur. Biophys. J.* **29**, 141–145 (2000).
- <sup>46</sup>P. R. C. Gascoyne, R. Pethig, J. P. H. Burt, and F. F. Becker, *Biochim. Biophys. Acta-Biomembr.* **1149**, 119–126 (1993).
- <sup>47</sup>A. Garner, G. Chen, N. Chen, V. Sridhara, J. Kolb, R. Swanson, S. Beebe, R. Joshi, and K. Schoenbach, *Biochem. Biophys. Res. Commun.* **362**, 139–144 (2007).
- <sup>48</sup>A. Salmanzadeh, H. Kittur, M. B. Sano, P. C. Roberts, E. M. Schmelz, and R. V. Davalos, *Biomicrofluidics* **6**, 024104 (2012).
- <sup>49</sup>L. Wu, L.-Y. L. Yung, and K.-M. Lim, *Biomicrofluidics* **6**, 014113 (2012).
- <sup>50</sup>F. Yang, X. Yang, H. Jiang, P. Bulkhauls, P. Wood, W. Hrshesky, and G. Wang, *Biomicrofluidics* **4**, 013204 (2010).